PERGAMON

International Journal of Heat and Mass Transfer 46 (2003) 127–138

International Journal of HEAT and MASS TRANSFER

www.elsevier.com/locate/ijhmt

Three-dimensional numerical simulation of natural convection in an inclined liquid-filled enclosure with an array of discrete heaters

S.K.W. Tou *, X.F. Zhang

School of Mechanical and Production Engineering, Nanyang Technological University, Nanyang Avenue North Spine (N3), Level 2, 63978 Singapore, Singapore

Received 15 May 2002

Abstract

A three-dimensional (3-D) numerical model is developed to investigate the effects of inclination on the heat transport processes in a liquid-filled rectangular enclosure of finite size. The interactions of flows tangential and normal to the heater surfaces in an inclined enclosure cause a slight oscillation in Nusselt number. Inclination has little effects on the average heat transfer characteristics except configurations close to the conduction case with heaters on top leading to a sharp decrease in Nusselt number. The critical Rayleigh number of 1708 is also observed in the present study regardless of inclinations. Heat transfer from discrete heaters is non-uniform. Maximum Nusselt number occurs at the heater leading edge and decreases towards the trailing edge. Correlations for the row average Nusselt number vs. Rayleigh number at various inclination angles are presented. By taking the average of the discrete heater array, the numerical results compared well with the empirical correlations obtained from a single heater plate in literature.

1. Introduction

The complex interactions of thermal and internal fluid flow fields in a finite-size, inclined fluid system confined by surrounding walls are a challenging subject faced by professional engineers. Fundamental studies have been initiated to gain a basic understanding on natural convection in rectangular enclosures with inclinations, most of which focus typically on a single hot wall and a cold wall [1,2]. The results show that the aspect ratio and inclination angle are of influential to the heat transfer processes. Study on the use of discrete heater arrays for heating liquids is considerably limited [3,4]. It is the objective of the present work to investigate the interactions of flows tangential and normal to the heater surfaces inclined at an arbitrary angle and their effects on the heat transport processes. Numerical results are then compared with those from literature and are used to develop correlations for practical use.

2. Model formulation and procedures

The enclosure geometry and parameters given in Fig. 1 and Table 1 are used in the present study. A three-dimensional (3-D) Cartesian coordinate system is then selected in such that it points positively upwards while the gravitational force acts downwards. The enclosure, filled with liquid, can be rotated about the horizontal X-axis to alter

* Corresponding author.
E-mail address: mkwtou@ntu.edu.sg (S.K.W. Tou).

0017-9310/03/$ - see front matter
PII: S0017-9310(02)00253-3

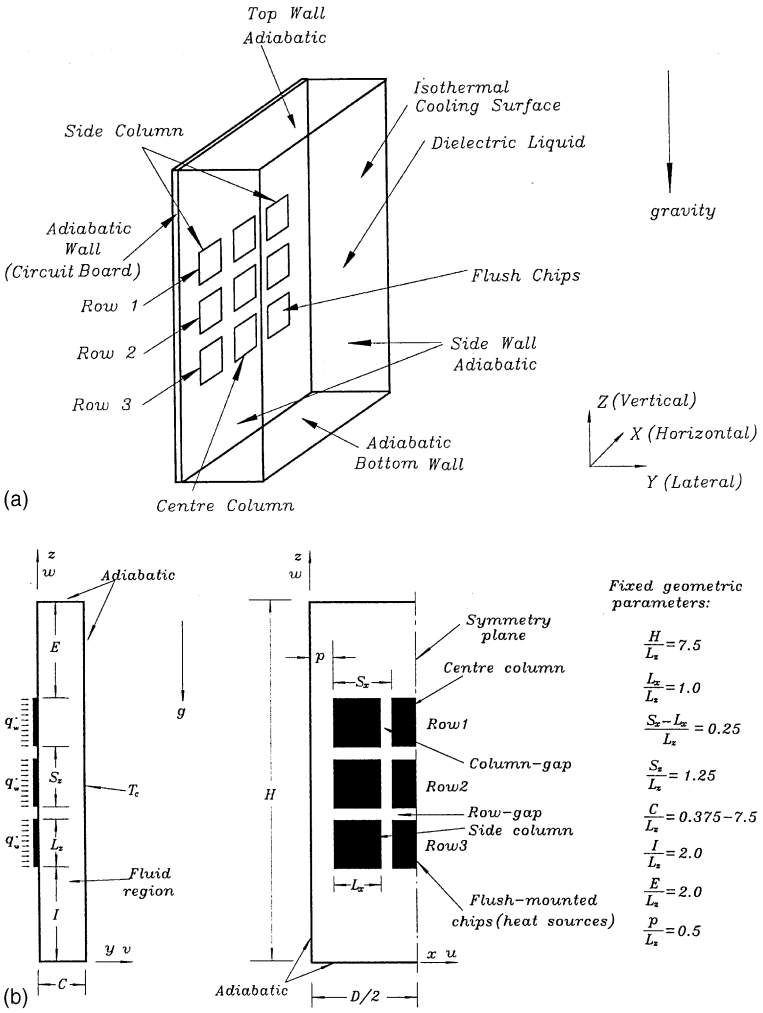

Fig. 1. The enclosure to be studied: (a) enclosure geometry and (b) sectional-view of enclosure with discrete heat sources.

Table 1
Summary of geometric parameters and model parameters

	Fixed geometric parameters $H = 95.3$ mm, $D = 57.2$ mm; $L_z = L_x = 12.7$ mm							Variable geometric parameter	
	H/L_z	L_x/L_z	$(S_x - L_x)/L_z$	S_x/L_z	I/L_z	E/L_z	b/L_z	Width aspect ratio, $A = H/C$	Inclination ϕ, °
(a) Geometric parameters	7.5	1.0	0.25	1.25	2.0	2.0	0.5	3, 7.5	0–360
	Prandtl number, Pr							Modified Rayleigh number Ra^*	
(b) Ranges of model parameters	5, 9							10–10^8	

its configuration set by the angle of inclinations. An array of 3×3 discrete heat sources is flush-mounted onto one of the sidewalls, while the opposite wall acts as a uniform cold surface. The remaining walls are insulated from surroundings.

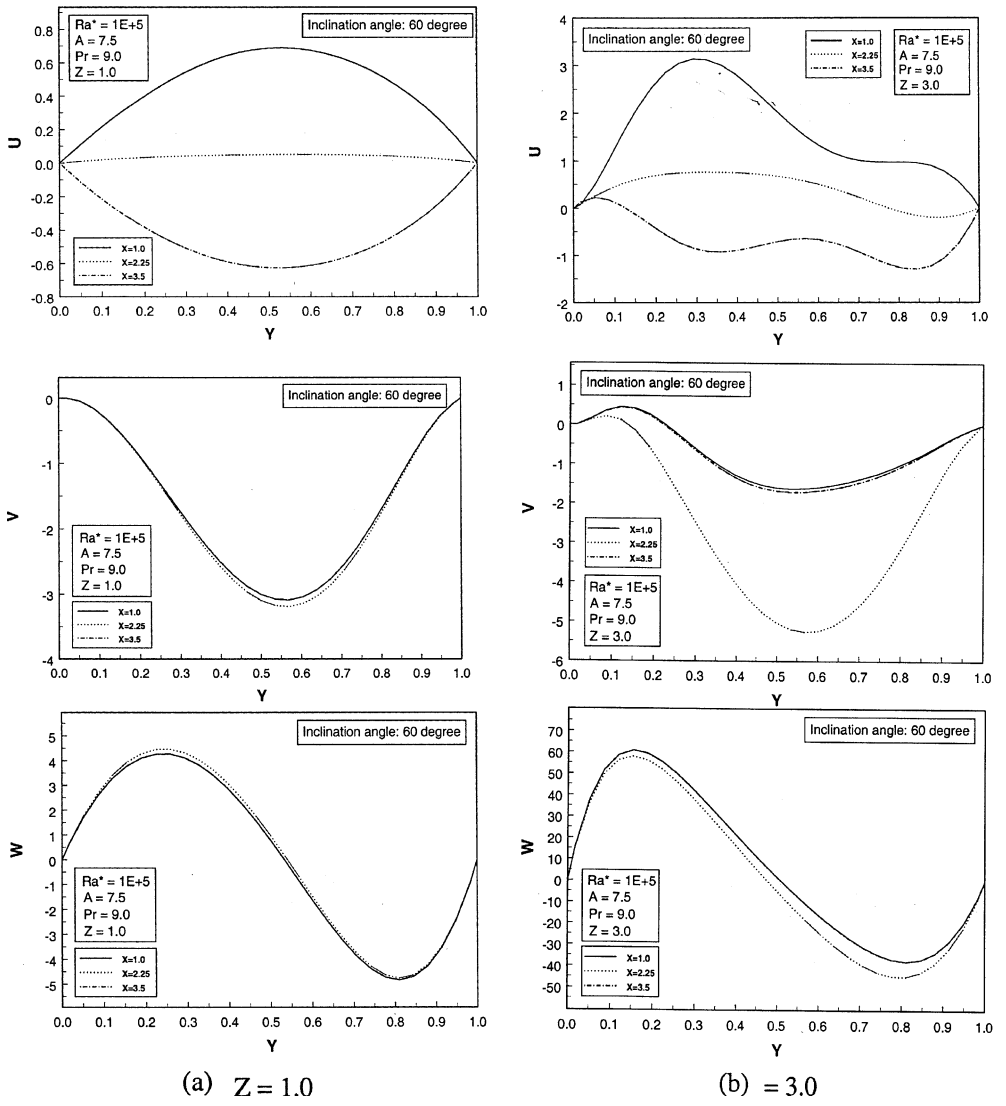

Fig. 2. U, V, W velocity profiles at different Z: (a) $Z = 1.0$; (b) $Z = 3.0$; (c) $Z = 5.5$ and (d) $Z = 6.5$.

2.1. Governing equations

Continuity:

$$\frac{\partial U}{\partial X}+\frac{\partial V}{\partial Y}+\frac{\partial W}{\partial Z}=0 \tag{1}$$

X-momentum:

$$U\frac{\partial U}{\partial X}+V\frac{\partial U}{\partial Y}+W\frac{\partial U}{\partial Z}=-\frac{\partial P}{\partial X}+Pr\left[\frac{\partial^2 U}{\partial X^2}+\frac{\partial^2 U}{\partial Y^2}+\frac{\partial^2 U}{\partial Z^2}\right] \tag{2}$$

Y-momentum:

$$U\frac{\partial V}{\partial X}+V\frac{\partial V}{\partial Y}+W\frac{\partial V}{\partial Z}=-\frac{\partial P}{\partial Y}+Pr\left[\frac{\partial^2 V}{\partial X^2}+\frac{\partial^2 V}{\partial Y^2}+\frac{\partial^2 V}{\partial Z^2}\right]+Ra^* Pr\,\theta\sin\phi \tag{3}$$

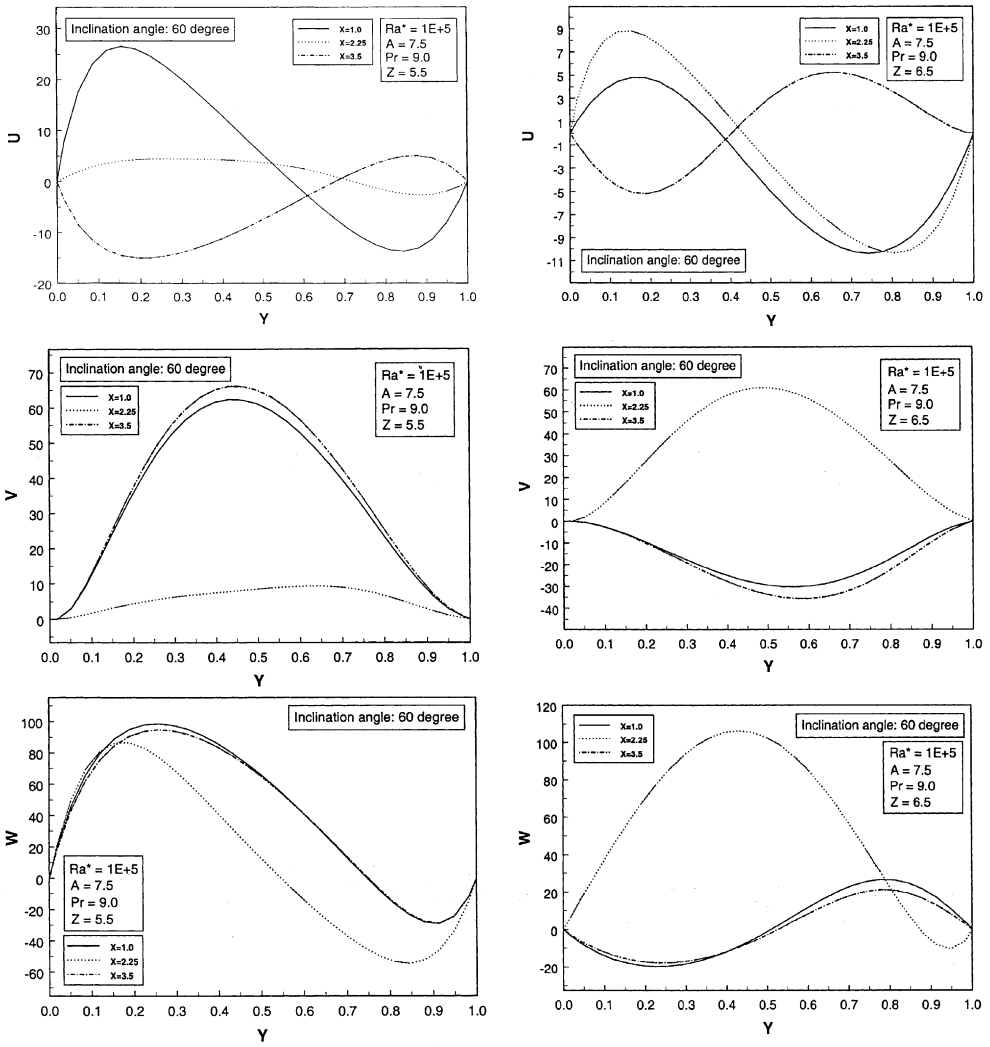

Fig. 2 (*continued*)

Z-momentum:

$$U\frac{\partial W}{\partial X}+V\frac{\partial W}{\partial Y}+W\frac{\partial W}{\partial Z}=-\frac{\partial P}{\partial Z}+Pr\left[\frac{\partial^2 W}{\partial X^2}+\frac{\partial^2 W}{\partial Y^2}+\frac{\partial^2 W}{\partial Z^2}\right]+Ra^{*}\,Pr\,\theta\cos\phi \tag{4}$$

Energy:

$$U\frac{\partial \theta}{\partial X}+V\frac{\partial \theta}{\partial Y}+W\frac{\partial \theta}{\partial Z}=\frac{\partial^2 \theta}{\partial X^2}+\frac{\partial^2 \theta}{\partial Y^2}+\frac{\partial^2 \theta}{\partial Z^2} \tag{5}$$

2.2. Boundary conditions

Constant heat flux is applied to the array of discrete heaters with the opposite wall acting as a cold wall. The remaining walls are assumed insulated from the surroundings. Then, the boundary conditions are as follows:

At $X = 0$: $P = 0, \quad \dfrac{\partial \theta}{\partial X} = 0, \quad U = V = W = 0$

At $X = \dfrac{D}{2L_z} = 2.25$: $\dfrac{\partial P}{\partial X} = 0, \quad \dfrac{\partial \theta}{\partial X} = 0, \quad U = \dfrac{\partial V}{\partial X} = \dfrac{\partial W}{\partial X} = 0$

At $Y = 0$: $\dfrac{\partial \theta}{\partial Y} = -1$ for the iso-flux region (heater)

$\dfrac{\partial \theta}{\partial Y} = 0$ for the adiabatic region (the rest) and $P = 0, \quad U = V = W = 0$

At $Y = \dfrac{C}{L_z} = 0.375 \to 7.5$: $P = 0, \quad \theta = 0, \quad U = V = W = 0$

At $Z = 0$ and $Z = \dfrac{H}{L_z} = 7.5$: $P = 0, \quad \dfrac{\partial \theta}{\partial Z} = 0, \quad U = V = W = 0$

The numerical procedures are the same as we reported previously [5].

3. Scale analysis and assessment of inclination effects

In order to assess the effects of inclination on the heat transfer processes, it is useful to apply the scale analysis. In the absence of a driving force, the X-momentum equation has little effects on the flow field through continuity coupling.

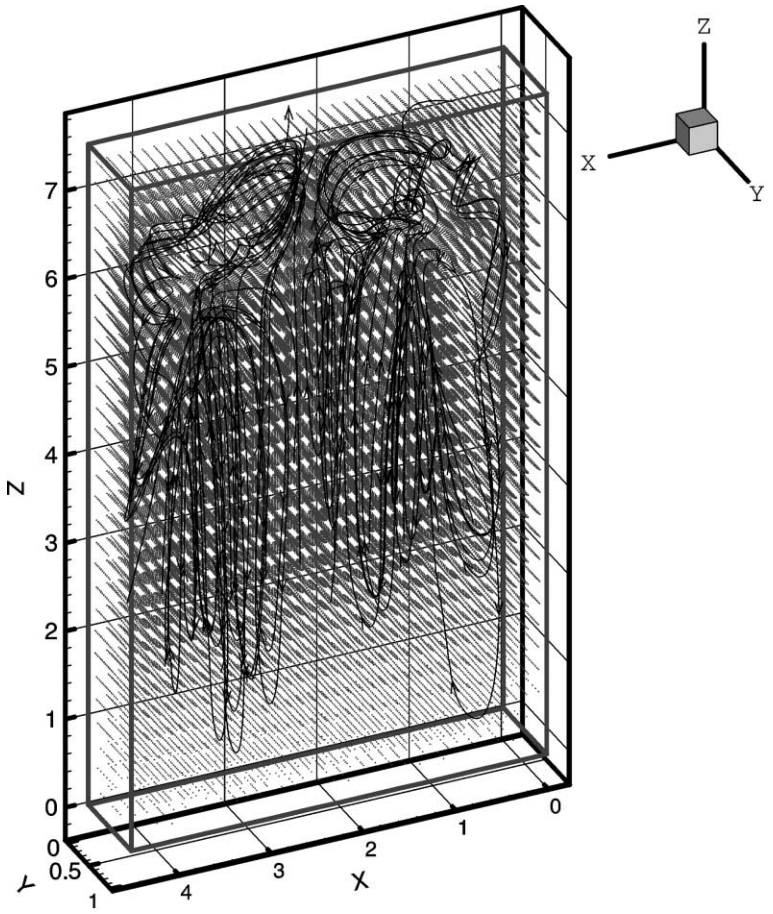

Fig. 3. 3-D velocity vector plot with streamline tracings at $\phi = 60°$: ($Ra^* = 10^5$, $Pr = 9$ and $A = 7.5$).

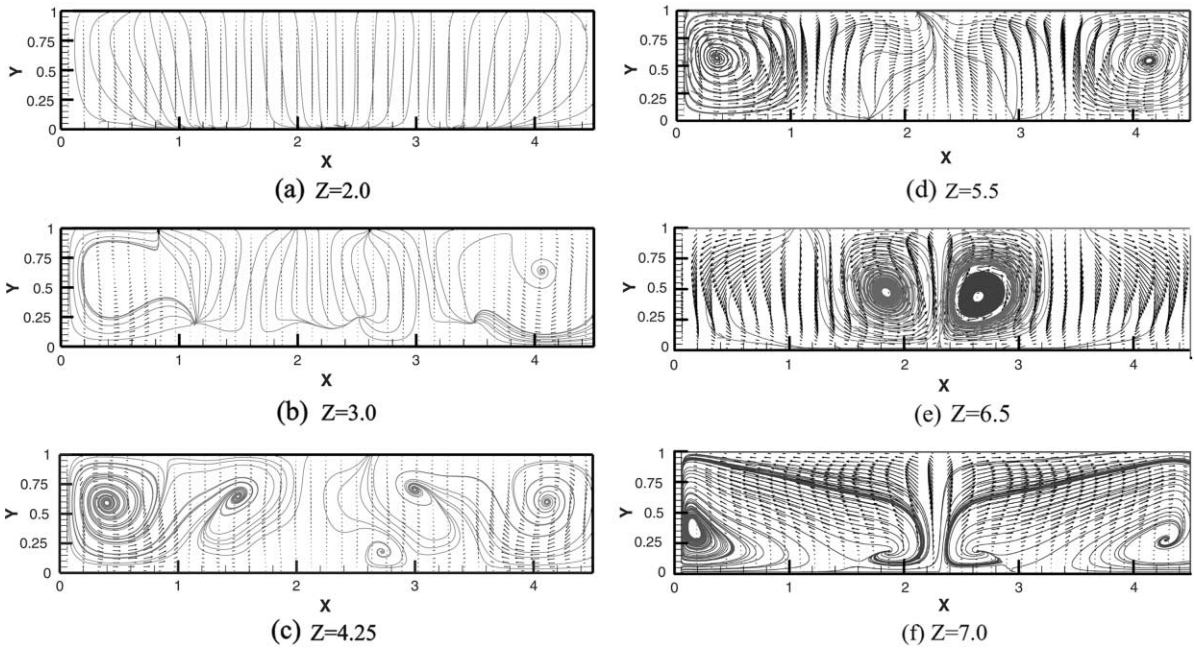

Fig. 4. 2-D velocity vectors with streamline tracings at X–Y planes with inclination angle 60° at selected Z locations for $Ra^* = 10^5$, $Pr = 0.9$ and $A = 7.5$ ($Y = 0.0$, hot wall; $Y = 1.0$, cold wall): (a) $Z = 2.0$; (b) $Z = 3.0$; (c) $Z = 4.25$; (d) $Z = 5.5$; (e) $Z = 6.5$ and (f) $Z = 7.0$.

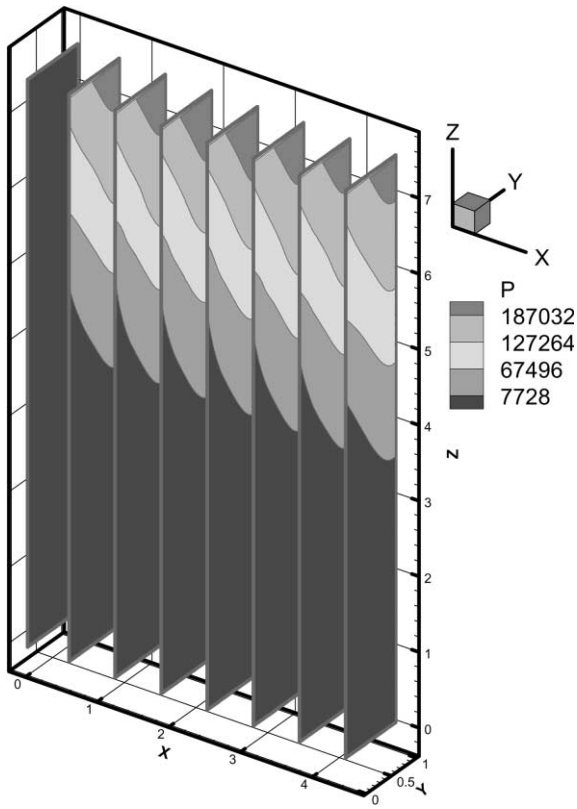

Fig. 5. Pressure contours at $\phi = 60°$ ($Ra^* = 10^5$, $Pr = 9$ and $A = 7.5$).

After eliminating the pressure gradient terms in the Y-momentum and Z-momentum equations and neglecting the minor terms, one obtains the dominate forces in the flow field as follows:

Inertia force	Viscous force	Buoyancy force
1	$1/Re$	$Ra^*(\cos\phi - \sin\phi)/PrRe^2$

It can be seen that buoyancy force is directly affected by inclination. The interaction of fluid flows tangential and normal to the walls comes in with inclinations. This renders 3-D flow fields of great complexity. In general, when there is a reduction of buoyancy in one direction, there is an increase in the other. From heat transfer point of view, this means when there is a reduction in convective heat transfer due to retardation of flow, there is a gain in heat transfer rate in the other stream, which strengthens. Such a loss and gain may be even out with little effects on the average heat transfer characteristics after taking the average. Furthermore the modification factor of $(\cos\phi - \sin\phi)$ is 0 ± 1.4, its effect is generally not dramatic. It does indicate the presence of a "negative buoyancy force". This situation corresponds to the case of conduction with heaters on top ($\phi = 270°$). Fluid on the upper half tends to move downwards and the heat transfer mechanism no longer depends on fluid motions.

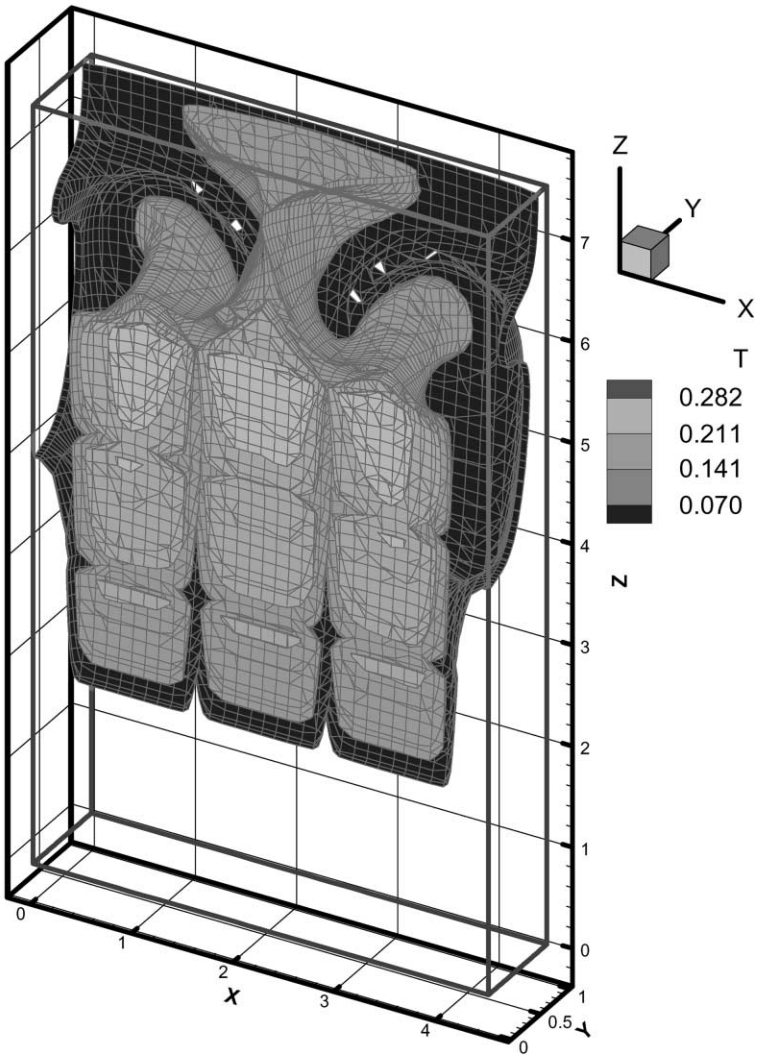

Fig. 6. Temperature field at $\phi = 60°$ ($Ra^* = 10^5$, $Pr = 9$ and $A = 7.5$).

4. Results and analyses

4.1. Dimensional nature of flow fields and pressure fields

The 3-D nature of the flow fields is presented in Fig. 2 for a test case with $\phi = 60°$, $Ra^* = 10^5$, $Pr = 9$ and $A = 7.5$. It shows the variations of velocity profiles across the enclosure at various elevated sections. The W-component is the strongest of all and represents the primary upward fluid motions in the enclosure. The strength of W-component is however very weak at the bottom region ($Z =\sim 1.0$) indicating that fluid is practically stagnant there. Adjacent to the hot wall, fluid driven by buoyancy force begins to accelerate from the bottom and set up the primary flow in the vertical upward direction. Maximum velocities across the heater array are attained in all three columns at the upper sections ($Z =\sim 5.5$). The W-component eventually bifurcates towards the ceiling and bottom noticeably in the enclosure central region (between $Y = 0.2$ and 0.8) and a flat $\sim$ profile takes shape whereby forming a pair of weak, rotating cells. On approaching the ceiling ($Z =\sim 6.5$), the rising plume begins to decelerate and flow across the enclosure towards the cold wall. Some of the fluids also bifurcate upon impingement with the ceiling, but they eventually sweep towards the cold wall by the bulk fluid motions. Adjacent to the cold wall, the primary flow is downward. As a result, two main opposite streams are formed in the enclosure being separated roughly by the mid-plane at centerline ($Y = 0.5$).

The velocity profiles for the U-component and V-component are also shown in Fig. 2. The U-component has strengthened considerably and is much stronger than the V component due to inclinations. They combine with the primary flow (W-component) and the resulting flow is a pair of rotating helical cells separated by the mid-plane.

The corresponding 3-D velocity vector plot with streamline tracings is given in Fig. 3. There are two major helical cells. The details of flow field near corners can also be seen. Two-dimensional (2-D) velocity vector plots with streamline tracings are also shown in Fig. 4. The pressure contour is presented in Fig. 5.

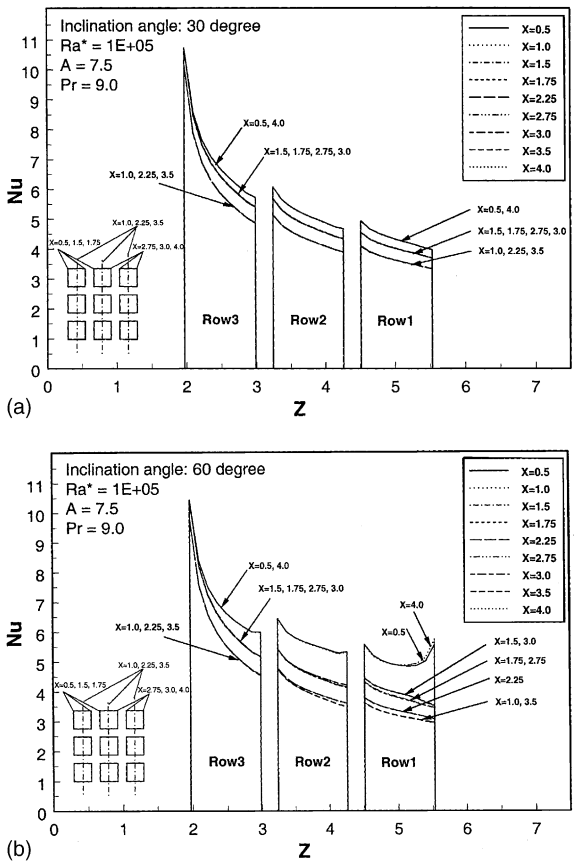

Fig. 7. Spatial variations of local Nusselt number at selected X locations: (a) $\phi = 30°$ and (b) $\phi = 60°$.

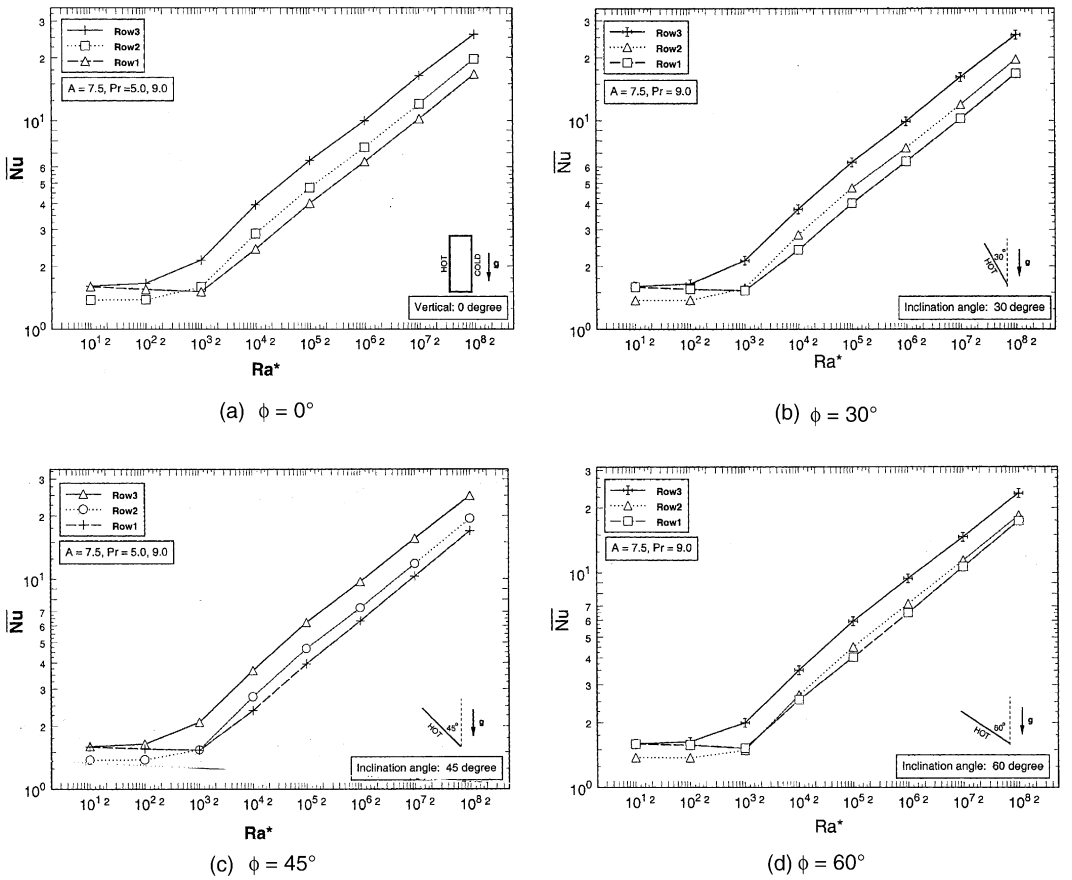

Fig. 8. The effects of inclination angle on heat transfer for each row of heaters: (a) $\phi = 0°$; (b) $\phi = 30°$; (c) $\phi = 45°$; (d) $\phi = 60°$; (e) $\phi = 90°$; (f) $\phi = 270°$ and (g) $\phi = 315°$.

4.2. Temperature fields and heat transfer characteristics

The temperature fields are illustrated in Fig. 6 at inclination angle $\phi = 60°$ with $Ra^* = 10^5$, $Pr = 9.0$ and $A = 7.5$. The maximum surface temperature (hot spot) on the discrete heater is seen to occur at the top row because fluid motion is weak and the local bulk fluid temperature is high in the ceiling. On the other hand, the heater surface temperature is the lowest at the bottom row where the local bulk fluid temperature is the lowest.

The spatial variations of local Nusselt number predicted by the present model at selected X locations are presented in Fig. 7 with $\phi = 30°$ and $60°$ respectively. It can be seen that the local Nusselt number decreases monotonously from the maximum at the leading edge towards the trailing edge in all heaters. The local Nusselt number is also non-uniform across the heater span and attains the maximum at the heater edges ($X = 0.5$). The same typical feature is also observed in vertical enclosures ($\phi = 90°$) [5].

4.3. The effects of inclination

Numerical results are obtained for a range of modified Rayleigh number from 10 to 10^8 and inclinations from 0° to 360°. Fig. 8 shows the variations of row average Nusselt number as a function of Rayleigh number over the full range of inclinations. For all cases, Nusselt number generally converges to about 1.5 as the Rayleigh number decreases to its low limit of 10, which is less than the critical value of 1708. Theoretically, Nusselt number assumes 1 for pure conduction with Rayleigh number approaches nil. In this conduction regime, the Nusselt number remains essentially unaltered until the Rayleigh number approaches the lower critical value of 1708. As the Rayleigh number passes the critical value there

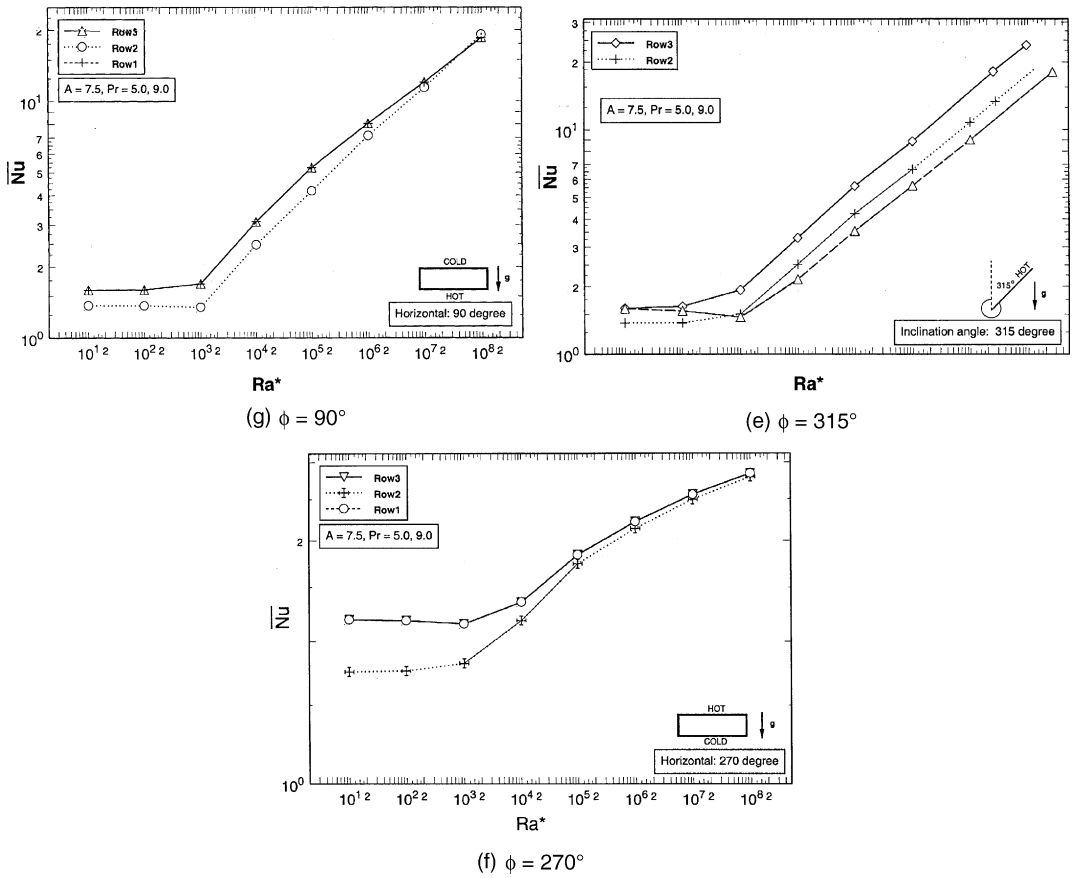

Fig. 8 (*continued*)

is clearly a sharp increase in heat transfer rate. The slopes of the curves change from zero to positive values. The increase in heat transfer rate is accomplished with the onset of natural convection.

Fig. 8(a)–(d) show the heat transfer characteristics with $\phi = 0°$, 30°, 45° and 60° respectively. They exhibit basically the same features. Fig. 8(g) shows the classical case of Bernard convection with heating from below ($\phi = 90°$). In this configuration, the row average Nusselt number is about the same for all columns. Fig. 8(f) illustrates the heat transfer case with heating on top ($\phi = 270°$). This configuration corresponds to conduction mode with Nusselt number typically around 1.5–2.5.

4.4. Numerical correlations and comparison of results

Numerical correlations for the row average Nusselt number as a function of Rayleigh number for each row are presented in Table 2 at various inclination angles. After taking average of all discrete heaters, the present results are ready to compare with the empirical correlations obtained from a single plate heater in literature. For an arbitrary angle of inclination, Bejan and others proposed the following empirical formula for an enclosure with uniform hot and cold surfaces opposite to each other [1]:

$$180 > \tau > 90, \quad \overline{Nu}_c = 1 + [\overline{Nu}_c(90) - 1]\sin\tau$$

$$90 > \tau > \tau^*, \quad \overline{Nu}_c = \overline{Nu}_c(90)(\sin\tau)^{1/4}$$

$$\tau^* > \tau > 0, \quad H/C < 10, \quad \overline{Nu}_c = \left[\frac{\overline{Nu}_c(90)}{\overline{Nu}_c(0)}(\sin\tau^*)^{1/4}\right]^{\tau/\tau^*}$$

Tilt angle τ is defined with respect to the horizon.

Table 2
Summary of correlations of $\overline{Nu_{L_{h,z}}}$ vs. $Ra_{L_{h,z}}$ at various inclination angles

$\phi = 30°$	
Row 1	$\overline{Nu_{L_{h,z}}} = 0.268\,Ra_{L_{h,z}}^{0.264}$
Row 2	$\overline{Nu_{L_{h,z}}} = 0.337\,Ra_{L_{h,z}}^{0.262}$
Row 3	$\overline{Nu_{L_{h,z}}} = 0.554\,Ra_{L_{h,z}}^{0.252}$
$\phi = 45°$	
Row 1	$\overline{Nu_{L_{h,z}}} = 0.250\,Ra_{L_{h,z}}^{0.270}$
Row 2	$\overline{Nu_{L_{h,z}}} = 0.317\,Ra_{L_{h,z}}^{0.266}$
Row 3	$\overline{Nu_{L_{h,z}}} = 0.549\,Ra_{L_{h,z}}^{0.251}$
$\phi = 60°$	
Row 1	$\overline{Nu_{L_{h,z}}} = 0.282\,Ra_{L_{h,z}}^{0.264}$
Row 2	$\overline{Nu_{L_{h,z}}} = 0.320\,Ra_{L_{h,z}}^{0.262}$
Row 3	$\overline{Nu_{L_{h,z}}} = 0.549\,Ra_{L_{h,z}}^{0.245}$
$\phi = 90°$	
Rows 1 and 3	$\overline{Nu_{L_{h,z}}} = 0.482\,Ra_{L_{h,z}}^{0.237}$
Row 2	$\overline{Nu_{L_{h,z}}} = 0.239\,Ra_{L_{h,z}}^{0.284}$
$\phi = 315°$ (heaters face down)	
Row 1	$\overline{Nu_{L_{h,z}}} = 0.240\,Ra_{L_{h,z}}^{0.261}$
Row 2	$\overline{Nu_{L_{h,z}}} = 0.284\,Ra_{L_{h,z}}^{0.265}$
Row 3	$\overline{Nu_{L_{h,z}}} = 0.387\,Ra_{L_{h,z}}^{0.270}$

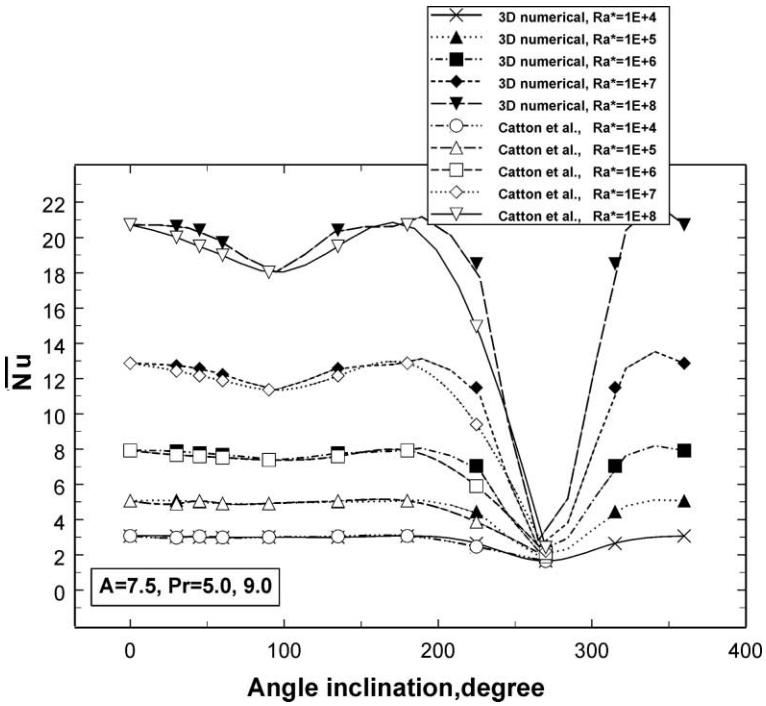

Fig. 9. The effects of inclination angle on heat transfer: comparison of numerical results and empirical correlations.

There is a local minimum Nusselt number at a special tilt angle τ^* depending on the aspect ratio. From Ref. [1], the local minimum occurs at $\tau^* = 65$ with $A = 7.5$.

Fig. 9 provides a comparison between these empirical correlations and the present study. There is a slight oscillation in Nusselt number as inclination changes. Such behavior is in-line with the prediction from scale analysis, which reveals the buoyancy force has been modified by a factor of $(\cos\phi - \sin\phi)$. Heat transfer characteristics are basically the same order of magnitude for all inclinations, except those in the range of $230° < \phi < 310°$ which corresponds to the conduction case of heating from top ($\phi = 270°$) and leads to a sharp decrease in Nusselt number. Fluid on the upper half tends to move downwards in the presence of a "negative buoyancy force".

5. Conclusions

Scale analysis is used to assess the effects of inclination on the heat transfer process within an enclosure. The predictions are in-line with the numerical results.

Complex flow fields and temperature fields are observed due to interactions of buoyancy forces tangential and normal to the heater surfaces. The critical Rayleigh number of 1708 is also observed in the present study regardless of inclinations.

Heat transfer from discrete heaters is non-uniform. Maximum Nusselt number occurs at the leading edge and decreases towards the trailing edge monotonously.

The heat transfer characteristics are about the same order of magnitude for all inclinations except in the range of $230° < \phi < 310°$. Which corresponds to or close to the conduction case with heaters on top ($\phi = 270°$) leading to a sharp decrease in Nusselt number. Outside this range, the Nusselt number oscillates slightly but appears to be bounded by a factor of $(\cos\phi - \sin\phi)$.

Correlations for the row average Nusselt number vs. Rayleigh number at various inclination angles are presented. Comparisons of results between the numerical model and empirical correlations from literature are encouraging.

References

[1] A. Bejan, Convection Heat Transfer, second ed., 1995.
[2] F.P. Incropera, Liquid cooling of electronic devices by single-phase convection, in: Wiley Series in Thermal Management of Microelectronic and Electronic Systems, 1999, pp. 90–124.
[3] H. Ozoe, H. Sayama, S.W. Churchill, Long rolls generated by natural convection in an inclined rectangular enclosure, Int. J. Heat Mass Transfer 26 (1983) 1427–1438.
[4] M.S. Polentini, S. Ramadhyani, F.P. Incropera, Single-phase thermosyphon cooling of an array of discrete heat sources in a rectangular cavity, Int. J. Heat Mass Transfer 36 (1993) 3983–3996.
[5] S.K.W. Tou, C.P. Tso, X.F. Zhang, 3-D numerical analysis of natural convection liquid cooling of a 3×3 heater array in rectangular enclosures, Int. J. Heat Mass Transfer 42 (1999) 3231–3244.